CHEMISTRY OF MATERIALS

Article

Cite This: *Chem. Mater.* 2018, 30, 2067−2073

pubs.acs.org/cm

Rapid Identification of the Layer Number of Large-Area Graphene on Copper

Zhikai Qi,[†,#] Xudong Zhu,[‡,§,#] Hongchang Jin,[†] Tiezhu Zhang,[∥] Xianghua Kong,[∥] Rodney S. Ruoff,[⊥] Zhenhua Qiao,[*,‡,§] and Hengxing Ji[*,†]

[†] Department of Materials Science and Engineering, CAS Key Laboratory of Materials for Energy Conversion, iChEM (Collaborative Innovation Center of Chemistry for Energy Materials), University of Science and Technology of China, Hefei, Anhui 230026, China

[‡] ICQD, Hefei National Laboratory for Physical Sciences at Microscale, and Synergetic Innovation Center of Quantum Information and Quantum Physics, University of Science and Technology of China, Hefei, Anhui 230026, China

[§] CAS Key Laboratory of Strongly-Coupled Quantum Matter Physics, and Department of Physics, University of Science and Technology of China, Hefei, Anhui 230026, China

[∥] School of Chemistry and Chemical Engineering, Hefei University of Technology, Hefei 230009, China

[⊥] Center for Multidimensional Carbon Materials, Institute for Basic Science Center at UNIST Campus, Ulsan 44919, Republic of Korea

Supporting Information

ABSTRACT: Chemical vapor deposition (CVD) on Cu foils emerged as an important method for preparing high-quality and large-area graphene films for practical applications. However, to date it remains challenging to rapidly identify the structural features, especially the layer numbers, of CVD-graphene directly on Cu substrate. Herein, we report an O_2-plasma-assisted approach for identifying the coverage, wrinkles, domain size, and layer number of large-area graphene films on Cu foils by optical microscopy. The wrinkles and grain boundaries of five-layer graphene can be observed with a grayscale increment of ∼23.4% per one graphene layer after O_2-plasma treatment for only 15 s, which allows for checking graphene on Cu foils with a sample size of 17 cm × 20 cm in a few minutes. The Raman spectroscopy and X-ray photoelectron spectroscopy presents a strong layer number dependence of both the plasma induced graphene defects and Cu oxides, which, as indicated by molecular dynamic simulation, is responsible for the improved image contrast as a result of the interaction between O-ions and graphene with different layer numbers. We expect that this O_2-plasma-assisted method would be applied to meter-scale samples if atmospheric-pressure plasma is used and therefore will be beneficial for the fast evaluation of CVD-graphene in both laboratory and industry.

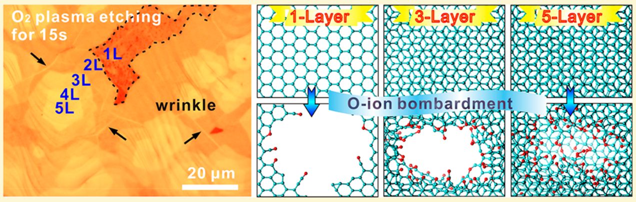

1. INTRODUCTION

Graphene is considered a promising material for applications in a variety of fields ranging from water-desaltation to microelectronics,[1−4] yet requires industrial-scale production, quality control, and processing techniques to convert lab-scale results to products.[5−8] Growing graphene on Cu foils by chemical vapor deposition (CVD) is an important approach for industrial-scale production, which is capable to provide graphene films with size of up to 300 cm × 30 cm and annual production capacities of 100,000 m^2.[9−12] It is known that the structure features of graphene film formed on Cu foils, for instance, the coverage, domain size, and layer number, dominate the physical properties and the downstream applications.[13,14] Therefore, a facile method that is able to identify the structure features of CVD-graphene film with lateral size of tens of centimeters in a couple of minutes at a low price is highly required.

The stacked layer number and domain size of graphene can be measured under optical microscope (OM)[15−18] and atomic force microscope (AFM),[19] and the defect concentration and distribution can be determined by Raman spectroscopy[20] when CVD-graphene is transferred to SiO_2/Si substrate. Though the SiO_2/Si substrate enables to effectively improve the signal/noise ratio for the above-mentioned analysis methods, the transfer process of graphene to SiO_2/Si wafer is time-consuming and costly. Scanning electron microscopy (SEM) can fast image micro- and nanoscale features of graphene on Cu substrates without transfer,[18] yet the sample size is limited in a few centimeters, and the instrument is expensive, making it unfit for the quality control of large samples.

OM allows for high-throughput characterization of graphene layers on SiO_2/Si substrate with a favored instrument cost. To date, direct observation of graphene on Cu foils without surface pretreatment using OM is extremely difficult because of the low

Received: December 28, 2017
Revised: March 9, 2018
Published: March 9, 2018

DOI: 10.1021/acs.chemmater.7b05377
Chem. Mater. 2018, 30, 2067−2073

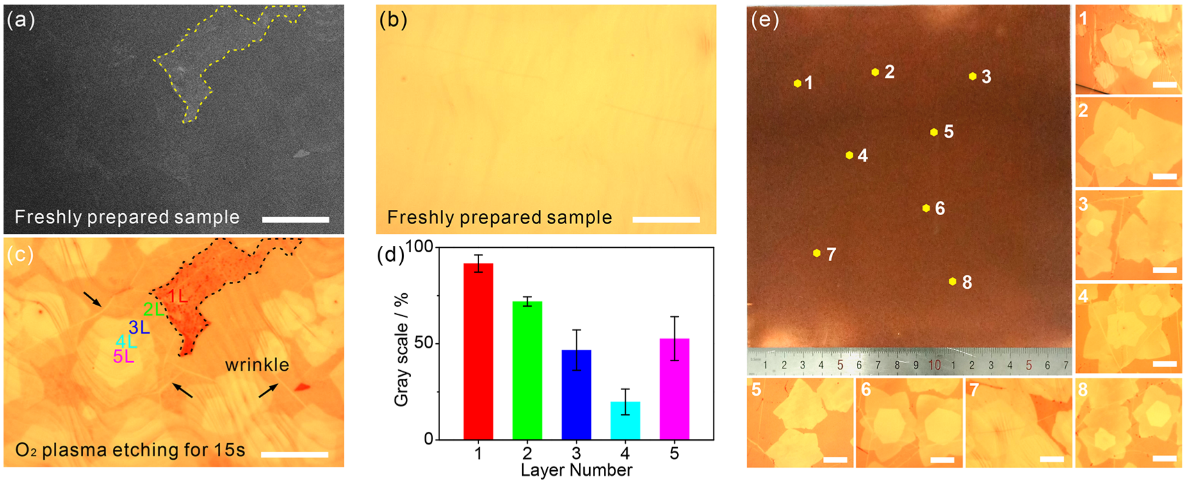

Figure 1. (a) Typical SEM image of the as-grown graphene on Cu foils showing a low contrast between the monolayer regions (marked with dashed yellow line) and multilayer regions. Optical images of graphene (b) before and (c) after O_2-plasma treatment for 15 s. The dashed black line marked the monolayer region, and the black arrows marked graphene wrinkles. The images shown in panels a, b, and c were taken from an identical area. (d) Grayscale of graphene domains after O_2-plasma treatment that was obtained from the optical images. (e) Photograph of a graphene covered Cu foil (17 cm × 20 cm) subjected to O_2-plasma treatment for 15 s and the OM images taken from different positions of the sample. All the scale bars are 20 μm.

contrast between the graphene covered and uncovered areas,[21] which is the key factor that greatly limits the application of OM. Therefore, great efforts have been taken to improve the contrast of graphene on Cu substrates. For instance, dark field optical imaging was reported to present graphene islands, cracks, and grain boundaries with high contrast dependent on the surface roughness of Cu substrate.[21] Surface oxidation by heating the Cu foil coated with graphene in air at above 160 °C increases the interference color contrast between graphene-covered Cu and uncovered Cu oxide.[22,23] Recently, ultraviolet irradiation with subsequent thermal annealing allows one to distinguish the layer number of graphene on Cu foils, which takes around 5 h for sample treatment (as long as that for transferring graphene to SiO_2/Si).[24] Therefore, the trade-off between the imaging contrast of graphene on Cu foils and the time efficiency has to be considered, and the OM based technique is still under development for direct imaging of graphene on Cu foils.

Herein, we demonstrate an O_2-plasma-assisted approach for the fast identification of large-area graphene on Cu foils using OM. The color contrast of graphene domains on Cu foils has been considerably enhanced after O_2-plasma treatment for only 15 s. The wrinkles and grain boundaries of five-layer graphene can be observed with a grayscale increment of ~23.4% per one graphene layer. The grayscale of graphene domains in optical image is inversely proportional to the layer numbers owing to the strong layer number dependence of graphene defects and Cu oxide overlayers induced by O_2-plasma according to the molecular dynamics (MD) simulation. This method was used to check graphene on Cu foils with a sample size of 17 cm × 20 cm in a few minutes.

2. RESULTS AND DISCUSSION

We prepared graphene film on Cu foils by CVD employing CH_4 as precursor (for details, see the Experimental Section). The SEM image (Figure 1a) of a freshly prepared sample shows an area with different contrast. The lightest area is covered with single layer graphene (marked with yellow dashed line); however, these features are invisible in the optical image (Figure 1b), which was taken from the same area as the SEM image (Figure 1a) and is in accordance with previous studies.[21] When the sample was treated with O_2-plasma for 15 s, flower-like graphene domains with different stacked layer numbers from 1 to 5 are distinguishable, and the wrinkles (marked with black arrows) are visible under OM (Figure 1c). These features fail to be captured either by SEM (Figure 1a) or OM (Figure 1b), as for the graphene without pretreatment. To quantitatively study the visibility of graphene domains with different layer numbers on Cu foils, we calculated the grayscale of graphene domains treated with O_2-plasma (Figure S1, see Supporting Information for the details) and plotted the values with respect to the stacked layer numbers (Figure 1d). The grayscale decreases when the layer number of graphene increases from 1 to 4, and the increment (contrast) is ~23.4% per one graphene layer. This value is much higher than that of the optical image of the graphene covered Cu sample that was placed at ambient conditions for four months (Figure S2). However, the thickest area at the center of the multilayer graphene domain usually shows a higher grayscale than that of the adjacent domain (with one layer less than the center area). Previous studies indicated that the color contrast and grayscale are dependent on the Cu oxide thickness under the graphene.[24] The center of a multilayer graphene domain is generally the nucleation site, where impurities in Cu and structural defects in graphene are accumulated.[25−27] The higher level of graphene defect at the domain center was proved by atomic layer deposition of Al_2O_3 (Figure S3).

We note that the plasma treatment process, including chamber pumping down, plasma treatment, and vacuum breaking, takes around 5 min, which is still considerably lower than previous works.[22,24] We performed the O_2-plasma treatment on a 17 cm × 20 cm graphene/Cu sample (Figure 1e), and the optical images (Figure 1e) acquired from different positions of the sample demonstrate graphene domains with different layer numbers and wrinkles with similar contrast as that of Figure 1c, indicating that the O_2-plasma treatment method is applicable to large-area samples for industrial-scale application.

DOI: 10.1021/acs.chemmater.7b05377
Chem. Mater. 2018, 30, 2067−2073

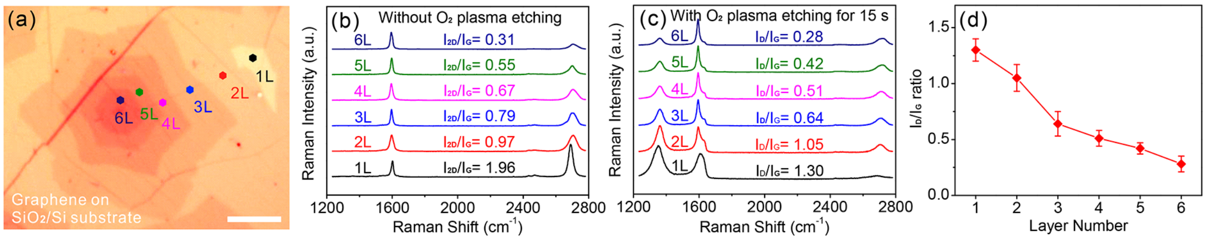

Figure 2. (a) Optical image of a six-layer graphene domain transferred onto a SiO_2/Si substrate. Scale bar: 10 μm. Raman spectra of graphene domains with different layer numbers (b) before and (c) after O_2-plasma treatment for 15 s. The intensities of the Raman bands in panels b and c are normalized to the G band intensity. (d) I_D/I_G ratio with respect to the layer numbers of graphene treated with O_2-plasma.

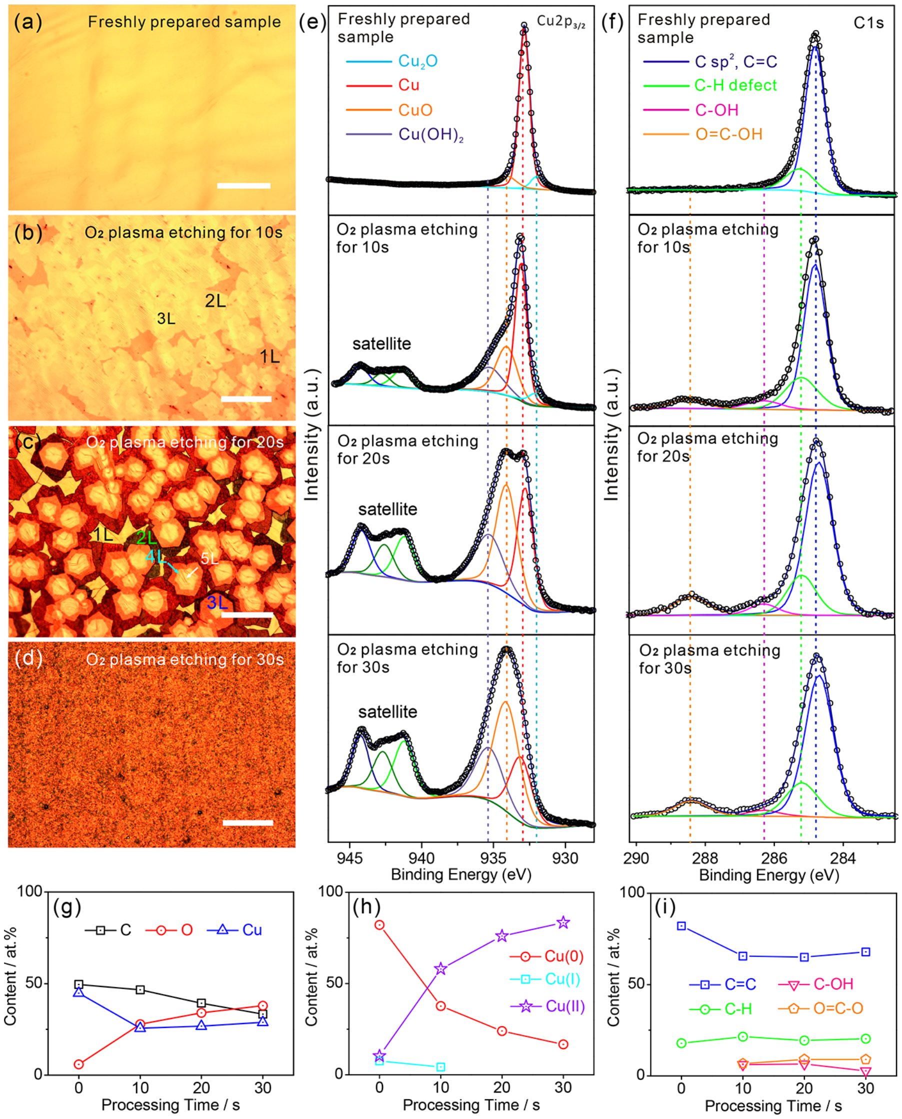

Figure 3. (a) Optical image of freshly prepared graphene on Cu foils, and (b–d) optical images of graphene with O_2-plasma treatment times of 10, 20, and 30 s. Scale bar: 20 μm. XPS spectra of (e) Cu $2p_{3/2}$ and (f) C 1s of graphene on Cu foils with different O_2-plasma treatment time. (g) Atom fractions of Cu, C, and O of the graphene-covered Cu at different O_2-plasma treatment times. (h,i) Atom fractions of Cu and C calculated by fitting the XPS in panels e and f, respectively.

Moreover, both the thermal annealing (Figure S4) and Ar-plasma treatment (Figure S5) improve the optical contrast of the one-layer graphene domain, yet not works for multilayer graphene domains. Therefore, the O_2-plasma treatment should be responsible for the enhanced optical contrast of graphene on Cu foils. O_2-plasma is widely used to etch graphene at room temperature as the high energy ionized O reacts with C atom in graphene lattice and leaves an atomic-size hole (defect), thus gradually removing graphene away from the substrate.[28−30] However, we observed a very low optical contrast of graphene on Cu–Ni alloy after O_2-plasma treatment (Figure S6). Unlike Cu metal, the Cu–Ni alloy is a corrosion resistive metal. These results indicate that the grayscale features of graphene in OM images is dependent on the Cu oxide thickness and that the Cu

DOI: 10.1021/acs.chemmater.7b05377
Chem. Mater. 2018, 30, 2067−2073

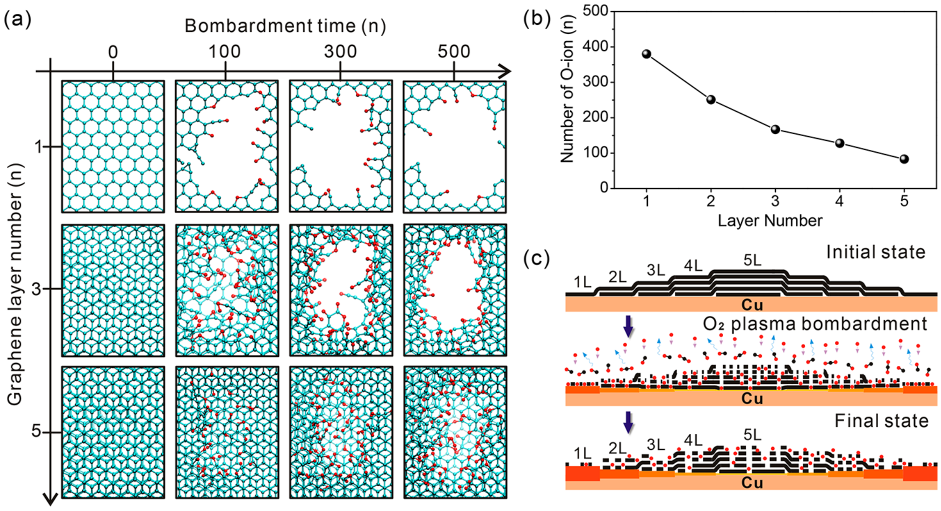

Figure 4. (a) Structure evolution of one-layer, three-layer, and five-layer graphene at different stages of O-ion bombardment obtained by MD simulation. (b) Number of O-ions that can penetrate through graphene layers and reach Cu substrate after 500 times of O-ion bombardment. (c) Schematic of the graphene structure and Cu oxide change during the O-ion bombardment.

oxide thickness should be closely associated with the graphene defects created by O_2-plasma.

To investigate the effect of O_2-plasma on graphene, the sample was carefully transferred to a SiO_2/Si substrate by PMMA method (for details, see the Experimental Section). The optical image (Figure 2a) shows an area with stacked graphene layer number of 1 to 6, which is distinguishable from the color contrasts. The Raman spectra of graphene with different layer numbers are shown in Figure 1b. Intensive G and 2D bands centered at ∼1590 and ∼2690 cm^{-1}, respectively, are clearly observed, and the intensity ratios of the 2D band to the G band (I_{2D}/I_G) decrease with the layer number of graphene. Nevertheless, the D bands (∼1360 cm^{-1}) are not observed, nicely indicating the high-quality graphene. When the graphene film was treated with O_2-plasma for 15 s, the D bands are shown in the Raman spectra (Figure 2c). The intensity ratios of the D band to the G band (I_D/I_G) decrease with the layer number of graphene (Figure 2d), proving that the O_2-plasma induced defect concentration is strongly dependent on the layer number. We note that each OM image presents an area of tens of micrometers in lateral size; therefore, the graphene domains with different layer numbers experienced the same O-ion bombardment during the plasma treatment. These results indicate that a thicker graphene layer contains a lower defect concentration, and we suggest that a higher defect concentration yields a thicker Cu oxide under the graphene layer.

To understand whether the optical contrast of graphene on Cu foils is dependent on the thickness of Cu oxide, we performed O_2-plasma treatment on graphene-covered Cu with processing times of 10, 20, and 30 s. The optical images of the samples exhibit that the contrast of graphene domains on Cu foils increases with the O_2-plasma treatment time ranging from 0 to 20 s (Figure 3a−c). However, when the processing time is 30 s, the graphene domains are invisible (Figure 3d). X-ray photoelectron spectroscopy (XPS) was applied to analyze the chemical composition of the graphene covered Cu. Both the Cu $2p_{3/2}$ and C 1s peaks of the freshly prepared sample display sharp bands locating at 932.8 and 284.8 eV, respectively, which can be assigned to Cu(0) and graphite-like sp^2-hybridized carbon (Figure 3e,f). These two bands get broader as the O_2-plasma treatment time increases (Figure 3e,f). Besides, new bands locating at a higher binding energy of the Cu $2p_{3/2}$ spectra (940−945 eV) and C 1s spectra (286−289 eV) are observed, and their intensities increase with the plasma treatment time (Figure 3e,f). The significant changes in the Cu $2p_{3/2}$ and C 1s peaks can be assigned to the formation of oxidized Cu and C species, respectively.[19,31,32] The atom fractions of different oxidation states of Cu and C were calculated by fitting the XPS data (Figure 3g−i). The atom fraction of C decreases, and that of O increases with the O_2-plasma treatment time. The atom fraction of Cu decreases when the O_2-plasma treatment time is <10 s and keeps almost unchanged with extended treatment (Figure 3g). Previous studies on the oxidation layer on Cu substrates indicated that Cu(I) was the initial product when Cu(0) was exposed to either O_2 at ambient conditions or O_2-plasma before being oxidized to Cu(II). Moreover, CuO layer can form only after the complete growth of Cu_2O layer at the Cu surface, which yielded an inner layer of Cu_2O and an outer layer of CuO on Cu.[32−34] Therefore, the atom fraction of Cu(II) increases and that of the Cu(0) decreases with the O_2-plasma treatment time. The atom fraction of Cu(I) is quite low and almost undetectable when the treatment time is more than 10 s. The very low factions of Cu(0) and Cu(I) in the XPS at O_2-plasma treatment time of >10 s can be assigned to the thick Cu(II) layer and low detection depth of XPS of few nanometers, whereas the sum of Cu(I) and Cu(II) contents increases with the O_2-plasma treatment time. However, the atom fractions of graphite-like sp^2 carbon of the O_2-plasma treated samples are lower than that of the freshly prepared sample due to the formation of oxidized carbon (Figure 3i). Interestingly, the C 1s spectrum of the sample after O_2-plasma treatment for 30 s still shows an intensive and narrow peak at 284.8 eV, indicating a considerable content of graphite-like sp^2-carbon (Figure 3i). These results suggest that the graphene film is partly oxidized after O_2-plasma treatment, and that there is quite a number of graphene laying on Cu foils when the O_2-plasma treatment time is 30 s, though the graphene film is invisible under OM (Figure 3d). Our combined OM and XPS analysis makes clear that both the color contrast of graphene and the Cu oxide increases with the O_2-plasma treatment time in the range of 0−20 s; thus, the formation of Cu oxide during O_2-plasma

DOI: 10.1021/acs.chemmater.7b05377
Chem. Mater. 2018, 30, 2067−2073

processing should be responsible for the visibility of graphene on Cu foils.

The experimental results presented in Figures 1−3 illustrate that 15 s of O_2-plasma treatment on graphene covered Cu enhances the color contrast of graphene domains, and the grayscale is inversely proportional to the layer number of graphene (Figure 1); O_2-plasma creates defects in graphene film, and the defect concentration measured by Raman scattering is inversely proportional to the stacked layer numbers (Figure 2). The color contrast of graphene domains is closely related to the amount of underneath Cu oxide (Figure 3). Therefore, the imaging contrast of graphene under OM should be strongly associated with the graphene defect and Cu oxide induced by O_2-plasma.

To rationalize the interplay among the color contrast, graphene defect concentration, and Cu oxide thickness, we performed MD simulation with a reactive force field (Figure 4a, see Supporting Information and Experimental Section for details).[35,36] We considered 500 O-ions continuously bombarding the graphene surface, and the interval time between two bombardments was 20 ps (see Supporting Information for details). Movies S1−S5 in Supporting Information present the structure evolution of the one-layer to five-layer graphene, respectively, during the O-ion bombarding process (500 O-ions with incidence energy of 20 eV[37]). Figure 4a presents the structure of one-layer, three-layer, and five-layer graphene at different stages of O-ion bombardment. Once the O-ion hits a carbon atom in graphene lattice, the energy of the O-ion will transfer to the graphene lattice. As a consequence, the carbon ring rearranges to form Stone−Wales defects, or the carbon atom is kicked off from the graphene lattices to leave vacancies in graphene lattice (Figure S7). Both processes leave defects in the graphene film. The oxygen atoms, after interacting with the carbon atoms, either could be absorbed in the graphene lattice to form C−O−C or O═C−O functional groups (Figure S8) or could form carbon oxide molecules that desorb from the graphene surface. Whereas once the O-ion meets the center of carbon ring, the graphene lattice deforms with a short relaxation time of around 20 ps, and the O-ion will penetrate through the top graphene layer to interact with Cu substrate or the layer underneath. Therefore, the O-ion bombardment generates oxygen-contained functional groups, Stone−Wales defects, and vacancies in graphene, and the O-ions can either (i) trap in the graphene lattices (to form functional groups), (ii) desorb from the surface (to form carbon oxide molecules), and (iii) penetrate through the top graphene layer. The probabilities of these three processes for O-ions are dependent on the incident energy as shown in Figure S9. The structure of graphene, after O-ion bombardments, is dependent on the layer number (Figure 4). The area, which is uncovered with graphene, increases as a function of the duration of bombardment. After the continuous bombardment of 500 O-ions, the one-layer graphene exposes the largest area of Cu substrate, and the number of O-ions that penetrate through graphene sheets is inversely proportional to the layer number of graphene (Figure 4b). The O-ions that reach the Cu substrate will generate Cu oxides; thus, the thickest Cu oxide layer can be found at the one-layer graphene covered area (Figure 4c), leading to different level of grayscale in the optical images. A prolonged O_2-plasma treatment can significantly damage the graphene layers, and the thicknesses of Cu oxide under graphene with different layer numbers are getting close; thus, the graphene domains are invisible (Figure 3d). This result is in accordance with our XPS measurement that the content of Cu(II) increases and reaches a plateau with the plasma treatment time (Figure 3g).

3. CONCLUSIONS

In conclusion, the optical contrast of graphene domains on Cu foils has been considerably enhanced after O_2-plasma treatment for only 15 s. The wrinkles and grain boundaries of five-layer graphene can be seen with a grayscale increment of ∼23.4% per one graphene layer. The improved optical contrast of graphene is owing to the strong layer number dependence of the plasma induced defects in graphene and consequently the amount of Cu oxides according to the MD simulation. We demonstrated that this method is applicable to large samples with lateral size of tens of centimeters. The O_2-plasma-assisted method allows for checking freshly prepared graphene on Cu foils within a few minutes and may be applicable to the samples with lateral size of meters if atmospheric-pressure plasma is used and therefore will be beneficial for fast and cost-effective evaluation of CVD-graphene in both laboratory and industry.

4. EXPERIMENTAL SECTION

4.1. Graphene Growth on Cu Foil. Multilayer graphene samples were fabricated by low-pressure CVD method using CH_4 as the carbon feedstock and H_2 as the reduction gas. Cu foils (25 μm thick, 99.8%, Alfa-Aesar stock #13382) were first dipped into the etchant (1:4 of HCl solution) for 5 h, followed by the ultrasonic cleaning using deionized (DI) water. Further, the pretreated Cu foil was first electrochemically polished at constant current of 5 A for 90 s[38] and then was cut into ∼3 cm × 5 cm pieces. This Cu foil was placed onto a flat quartz substrate, then together they were loaded into a hot wall tube furnace (Hefei Kejing Company OTF-1200x), and the reaction chamber was evacuated to ∼1 mTorr. For a typical growth process, the substrate was heated to 1040 °C at the rate of 25 °C/min under vacuum and then annealed at this temperature under 5−10 sccm H_2 with a pressure of 65−120 mTorr for 30 min. Graphene growth was typically achieved at 1040 °C using a CH_4/H_2 ratio of 1:5 and CH_4 flow of 1−2 sccm with a pressure of 13−28 mTorr for 30 min. After growth, we turned off the furnace, and the substrate was cooled in the same atmosphere.

4.2. Plasma-Assisted Optical Identification of Layer Number of Graphene on Cu Foils. Freshly prepared graphene samples on Cu foils were subjected to plasma etching using an AST PS−PJ Plasma Surface Treatment System (AST Products Inc., USA). The chamber was evacuated to ∼0.1 Torr and then filled with 15−30 sccm O_2 or Ar to ∼0.3 Torr. Typical plasma treatment was performed for several seconds at 10−30 W RF. The graphene samples after Ar-plasma treatments were placed on a hot plate and heated at 300 °C in air for several seconds, whereby only monolayer areas can be optically observed. The multilayer graphene with O_2 plasma etching can directly identify its layer numbers under OM.

4.3. Graphene Transfer. The multilayer graphene on Cu foils was spin-coated with a supporting polymer film (poly(methyl methacrylate), PMMA, 182265-Sigma-Aldrich) at 3000 rpm for 40 s. Then, the PMMA/graphene/Cu sheet was floated on the etchant (0.5 M of ammonium persulfate, $(NH_4)_2S_2O_8$). After the Cu catalyst was removed thoroughly, the graphene supported by PMMA was rinsed in DI water to wash off chemical residue and then transferred onto a SiO_2 (285 nm)/Si wafer. Finally, the supporting PMMA film was removed by acetone.

4.4. Characterization. Optical microscope (Nikon Eclipse LV100ND, Japan) was used to identify graphene on Cu foils before and after thermal annealing or/and plasma etching. The SEM images were obtained with a JSM-2100F (JEOL Ltd.) operated at 10.0 kV. The Raman spectra of graphene on SiO_2/Si substrate were measured by Renishaw inVia with a 532 nm laser and 50× objective lens. XPS analysis was conducted with a Thermo ESCALAB 250 instrument using a magnesium anode (monochromatic $K\alpha$ X-rays at 1486.6 eV) as the source.

4.5. Calculation. MD simulations were performed using the reactive force field (ReaxFF). The theoretical model consists of an incident oxygen ion placed 2 nm away from the graphene and a 5.2 nm × 4 nm multilayer graphene sheet varied from monolayer to five-layer (817 C atoms per layer, AB-stacking). Periodic boundary conditions were applied along the graphene basal plane to simulate an infinite sheet of graphene. The impact site is supposed to be random in both one-time and continuous bombardment, and the incident angle is assumed to be perpendicular to the graphene.[36]

■ ASSOCIATED CONTENT

Supporting Information

The Supporting Information is available free of charge on the ACS Publications website at DOI: 10.1021/acs.chemmater.7b05377.

Details of MD simulation, grayscale analysis and additional figures (PDF)

Videos showing the process of O-ion bombardment on graphene (AVI, AVI, AVI, AVI, AVI)

■ AUTHOR INFORMATION

Corresponding Authors

*E-mail: jihengx@ustc.edu.cn.
*E-mail: qiao@ustc.edu.cn.

ORCID

Hengxing Ji: 0000-0003-2851-9878

Author Contributions

[#]These authors contributed equally to this work.

Notes

The authors declare no competing financial interest.

■ ACKNOWLEDGMENTS

We appreciate funding support from the Natural Science Foundation of China (21373197), support from the 100 Talents Program of the Chinese Academy of Sciences, USTC Startup, the Fundamental Research Funds for the Central Universities (WK2060140003), and iChEM. X.H.K. thanks the Natural Science Foundation of China (21503064) and the Anhui Provincial Natural Science Foundation for support (Grant 1508085QE103).

■ REFERENCES

(1) Surwade, S. P.; Smirnov, S. N.; Vlassiouk, I. V.; Unocic, R. R.; Veith, G. M.; Dai, S.; Mahurin, S. M. Water desalination using nanoporous single-layer graphene. *Nat. Nanotechnol.* **2015**, *10*, 459−464.

(2) Sun, J.; Chen, Z.; Yuan, L.; Chen, Y.; Ning, J.; Liu, S.; Ma, D.; Song, X.; Priydarshi, M. K.; Bachmatiuk, A.; Rümmeli, M. H.; Ma, T.; Zhi, L.; Huang, L.; Zhang, Y.; Liu, Z. Direct Chemical-Vapor-Deposition-Fabricated, Large-Scale Graphene Glass with High Carrier Mobility and Uniformity for Touch Panel Applications. *ACS Nano* **2016**, *10*, 11136−11144.

(3) Sun, J.; Chen, Y.; Priydarshi, M. K.; Gao, T.; Song, X.; Zhang, Y.; Liu, Z. Graphene Glass from Direct CVD Routes: Production and Applications. *Adv. Mater.* **2016**, *28*, 10333−10339.

(4) Zang, J.; Ryu, S.; Pugno, N.; Wang, Q.; Tu, Q.; Buehler, M. J.; Zhao, X. Multifunctionality and control of the crumpling and unfolding of large-area graphene. *Nat. Mater.* **2013**, *12*, 321−325.

(5) Xu, X.; Zhang, Z.; Dong, J.; Yi, D.; Niu, J.; Wu, M.; Lin, L.; Yin, R.; Li, M.; Zhou, J.; Wang, S.; Sun, J.; Duan, X.; Gao, P.; Jiang, Y.; Wu, X.; Peng, H.; Ruoff, R. S.; Liu, Z.; Yu, D.; Wang, E.; Ding, F.; Liu, K. Ultrafast epitaxial growth of metre-sized single-crystal graphene on industrial Cu foil. *Sci. Bull.* **2017**, *62*, 1074−1080.

(6) Ma, T.; Ren, W.; Zhang, X.; Liu, Z.; Gao, Y.; Yin, L.-C.; Ma, X.-L.; Ding, F.; Cheng, H.-M. Edge-controlled growth and kinetics of single-crystal graphene domains by chemical vapor deposition. *Proc. Natl. Acad. Sci. U. S. A.* **2013**, *110*, 20386−20391.

(7) Bae, S.; Kim, H.; Lee, Y.; Xu, X.; Park, J.-S.; Zheng, Y.; Balakrishnan, J.; Lei, T.; Ri Kim, H.; Song, Y. I.; Kim, Y.-J.; Kim, K. S.; Ozyilmaz, B.; Ahn, J.-H.; Hong, B. H.; Iijima, S. Roll-to-roll production of 30-in. graphene films for transparent electrodes. *Nat. Nanotechnol.* **2010**, *5*, 574−578.

(8) Chen, X.; Wu, B.; Liu, Y. Direct preparation of high quality graphene on dielectric substrates. *Chem. Soc. Rev.* **2016**, *45*, 2057−2074.

(9) Zhu, Y. W.; Ji, H. X.; Cheng, H. M.; Ruoff, R. S. Mass production and industrial applications of graphene materials. *Natl. Sci. Rev.* **2018**, *0*, 1−12.

(10) Fang, W.; Hsu, A. L.; Song, Y.; Kong, J. A review of large-area bilayer graphene synthesis by chemical vapor deposition. *Nanoscale* **2015**, *7*, 20335−20351.

(11) Ta, H. Q.; Perello, D. J.; Duong, D. L.; Han, G. H.; Gorantla, S.; Nguyen, V. L.; Bachmatiuk, A.; Rotkin, S. V.; Lee, Y. H.; Rummeli, M. H. Stranski-Krastanov and Volmer-Weber CVD Growth Regimes To Control the Stacking Order in Bilayer Graphene. *Nano Lett.* **2016**, *16*, 6403−6410.

(12) Han, J.; Lee, J. Y.; Yeo, J. S. Large-area layer-by-layer controlled and fully bernal stacked synthesis of graphene. *Carbon* **2016**, *105*, 205−213.

(13) Fang, W.; Hsu, A. L.; Song, Y.; Birdwell, A. G.; Amani, M.; Dubey, M.; Dresselhaus, M. S.; Palacios, T.; Kong, J. Asymmetric Growth of Bilayer Graphene on Copper Enclosures Using Low-Pressure Chemical Vapor Deposition. *ACS Nano* **2014**, *8*, 6491−6499.

(14) Li, Z.; Zhang, W.; Fan, X.; Wu, P.; Zeng, C.; Li, Z.; Zhai, X.; Yang, J.; Hou, J. Graphene Thickness Control via Gas-Phase Dynamics in Chemical Vapor Deposition. *J. Phys. Chem. C* **2012**, *116*, 10557−10562.

(15) Yan, Z.; Liu, Y.; Ju, L.; Peng, Z.; Lin, J.; Wang, G.; Zhou, H.; Xiang, C.; Samuel, E. L. G.; Kittrell, C.; Artyukhov, V. I.; Wang, F.; Yakobson, B. I.; Tour, J. M. Large Hexagonal Bi- and Trilayer Graphene Single Crystals with Varied Interlayer Rotations. *Angew. Chem.* **2014**, *126*, 1591−1595.

(16) Roddaro, S.; Pingue, P.; Piazza, V.; Pellegrini, V.; Beltram, F. The Optical Visibility of Graphene: Interference Colors of Ultrathin Graphite on SiO2. *Nano Lett.* **2007**, *7*, 2707−2710.

(17) Blake, P.; Hill, E. W.; Castro Neto, A. H.; Novoselov, K. S.; Jiang, D.; Yang, R.; Booth, T. J.; Geim, A. K. Making graphene visible. *Appl. Phys. Lett.* **2007**, *91*, 063124.

(18) Hao, Y.; Wang, L.; Liu, Y.; Chen, H.; Wang, X.; Tan, C.; Nie, S.; Suk, J. W.; Jiang, T.; Liang, T.; Xiao, J.; Ye, W.; Dean, C. R.; Yakobson, B. I.; McCarty, K. F.; Kim, P.; Hone, J.; Colombo, L.; Ruoff, R. S. Oxygen-activated growth and bandgap tunability of large single-crystal bilayer graphene. *Nat. Nanotechnol.* **2016**, *11*, 426−431.

(19) Luo, D.; You, X.; Li, B.-W.; Chen, X.; Park, H. J.; Jung, M.; Ko, T. Y.; Wong, K.; Yousaf, M.; Chen, X.; Huang, M.; Lee, S. H.; Lee, Z.; Shin, H.-J.; Ryu, S.; Kwak, S. K.; Park, N.; Bacsa, R. R.; Bacsa, W.; Ruoff, R. S. Role of Graphene in Water-Assisted Oxidation of Copper in Relation to Dry Transfer of Graphene. *Chem. Mater.* **2017**, *29*, 4546−4556.

(20) Chen, J.; Han, Y.; Kong, X.; Deng, X.; Park, H. J.; Guo, Y.; Jin, S.; Qi, Z.; Lee, Z.; Qiao, Z.; Ruoff, R. S.; Ji, H. The Origin of Improved Electrical Double-Layer Capacitance by Inclusion of Topological Defects and Dopants in Graphene for Supercapacitors. *Angew. Chem., Int. Ed.* **2016**, *55*, 13822−13827.

(21) Kong, X. H.; Ji, H. X.; Piner, R. D.; Li, H. F.; Magnuson, C. W.; Tan, C.; Ismach, A.; Chou, H.; Ruoff, R. S. Non-destructive and rapid evaluation of chemical vapor deposition graphene by dark field optical microscopy. *Appl. Phys. Lett.* **2013**, *103*, 043119.

(22) Jia, C.; Jiang, J.; Gan, L.; Guo, X. Direct Optical Characterization of Graphene Growth and Domains on Growth Substrates. *Sci. Rep.* **2012**, *2*, 707.

(23) Gan, L.; Zhang, H.; Wu, R.; Ding, Y.; Sheng, P.; Luo, Z. Controlled removal of monolayers for bilayer graphene preparation and visualization. *RSC Adv.* **2015**, *5*, 25471−25476.

(24) Cheng, Y.; Song, Y.; Zhao, D.; Zhang, X.; Yin, S.; Wang, P.; Wang, M.; Xia, Y.; Maruyama, S.; Zhao, P.; Wang, H. Direct Identification of Multilayer Graphene Stacks on Copper by Optical Microscopy. *Chem. Mater.* **2016**, *28*, 2165−2171.

(25) Luo, B.; Whelan, P. R.; Shivayogimath, A.; Mackenzie, D. M. A.; Bøggild, P.; Booth, T. J. Copper Oxidation through Nucleation Sites of Chemical Vapor Deposited Graphene. *Chem. Mater.* **2016**, *28*, 3789−3795.

(26) Zhao, H.; Lin, Y.-C.; Yeh, C.-H.; Tian, H.; Chen, Y.-C.; Xie, D.; Yang, Y.; Suenaga, K.; Ren, T.-L.; Chiu, P.-W. Growth and Raman Spectra of Single-Crystal Trilayer Graphene with Different Stacking Orientations. *ACS Nano* **2014**, *8*, 10766−10773.

(27) Kwak, J.; Jo, Y.; Park, S.-D.; Kim, N. Y.; Kim, S.-Y.; Shin, H.-J.; Lee, Z.; Kim, S. Y.; Kwon, S.-Y. Oxidation behavior of graphene-coated copper at intrinsic graphene defects of different origins. *Nat. Commun.* **2017**, *8*, 1549.

(28) Hui, L. S.; Whiteway, E.; Hilke, M.; Turak, A. Effect of post-annealing on the plasma etching of graphene-coated-copper. *Faraday Discuss.* **2014**, *173*, 79−93.

(29) Lee, G.; Kim, J.; Kim, K.; Han, J. W. Precise control of defects in graphene using oxygen plasma. *J. Vac. Sci. Technol., A* **2015**, *33*, 060602.

(30) Gokus, T.; Nair, R. R.; Bonetti, A.; Böhmler, M.; Lombardo, A.; Novoselov, K. S.; Geim, A. K.; Ferrari, A. C.; Hartschuh, A. Making Graphene Luminescent by Oxygen Plasma Treatment. *ACS Nano* **2009**, *3*, 3963−3968.

(31) Yang, D.; Velamakanni, A.; Bozoklu, G.; Park, S.; Stoller, M.; Piner, R. D.; Stankovich, S.; Jung, I.; Field, D. A.; Ventrice, C. A.; Ruoff, R. S. Chemical analysis of graphene oxide films after heat and chemical treatments by X-ray photoelectron and Micro-Raman spectroscopy. *Carbon* **2009**, *47*, 145−152.

(32) Platzman, I.; Brener, R.; Haick, H.; Tannenbaum, R. Oxidation of Polycrystalline Copper Thin Films at Ambient Conditions. *J. Phys. Chem. C* **2008**, *112*, 1101−1108.

(33) Bellakhal, N.; Draou, K.; Brisset, J. L. Electrochemical investigation of copper oxide films formed by oxygen plasma treatment. *J. Appl. Electrochem.* **1997**, *27*, 414−421.

(34) Iijima, J.; Lim, J. W.; Hong, S. H.; Suzuki, S.; Mimura, K.; Isshiki, M. Native oxidation of ultra high purity Cu bulk and thin films. *Appl. Surf. Sci.* **2006**, *253*, 2825−2829.

(35) Chenoweth, K.; van Duin, A. C. T.; Goddard, W. A. ReaxFF Reactive Force Field for Molecular Dynamics Simulations of Hydrocarbon Oxidation. *J. Phys. Chem. A* **2008**, *112*, 1040−1053.

(36) Bai, Z.; Zhang, L.; Liu, L. Bombarding Graphene with Oxygen Ions: Combining Effects of Incident Angle and Ion Energy To Control Defect Generation. *J. Phys. Chem. C* **2015**, *119*, 26793−26802.

(37) Olthoff, J. K.; Van Brunt, R. J.; Radovanov, S. B.; Rees, J. A.; Surowiec, R. Kinetic-energy distributions of ions sampled from argon plasmas in a parallel-plate, radio-frequency reference cell. *J. Appl. Phys.* **1994**, *75*, 115−125.

(38) Zhang, B.; Lee, W. H.; Piner, R.; Kholmanov, I.; Wu, Y.; Li, H.; Ji, H.; Ruoff, R. S. Low-Temperature Chemical Vapor Deposition Growth of Graphene from Toluene on Electropolished Copper Foils. *ACS Nano* **2012**, *6*, 2471−2476.